Global Dynamics of Charged Dust Particles in Planetary Magnetospheres

J. E. Howard
Center for Integrated Plasma Studies, Campus Box 0390, University of Colorado, Boulder, Colorado 80309

M. Horányi and G. R. Stewart
Laboratory for Atmospheric and Space Physics, Campus Box 0392, University of Colorado, Boulder, Colorado 80309

(Received 21 June 1999)

We study the global stability of charged dust grains orbiting an axisymmetric planet. The corotating magnetic field and induced electric field are described in an inertial frame using the magnetic stream function and a two-dimensional effective potential U^e, parametrized by the conserved angular momentum p_ϕ. Stable equilibria form the centers of complex potential wells, so that a particle which loses local stability can still be trapped globally. Applying the results to Saturn, we find that nonequatorial "halo" orbits are dominated by positively charged grains.

PACS numbers: 96.30.Wr, 45.20.Jj, 96.35.Kx

The dynamics of planetary rings continues to present surprises and challenges to celestial mechanics. Earlier Voyager, Ulysses, and Galileo observations revealed complex dust rings around all four outer gaseous planets; now the impending visit of the Cassini orbiter promises to yield even more detailed information on Saturn's magnetosphere. Although much work has been done on the stability of charged dust grains [1–6], these studies have been largely limited to negatively charged particles in prograde (corotating) equatorial orbits [1], or neglect perturbations transverse to the equatorial plane [3]. Furthermore, there are ample theoretical and experimental grounds [7] for the presence of positively charged grains as well. In this Letter we carry out local and global stability analyses for both positively and negatively charged grains, in both prograde and retrograde orbits about an axisymmetric planet, an excellent approximation for Saturn and a fair approximation for Jupiter. We shall be primarily concerned with equatorial orbits about Saturn; future publications will include applications to Jupiter's rings, as well as the rather complicated dynamics of nonequatorial equilibria [8]. Our physical model includes Keplerian gravity, corotating planetary magnetic field (taken to be an aligned centered dipole) with concomitant induced electric field. For single particle dynamics over the short time scales envisioned here, it is reasonable to neglect radiation pressure, plasma drag, planetary oblateness, charge fluctuations, and collective effects [5]. The combined gravitational, magnetic, and electric forces are conveniently modeled by a two-dimensional effective potential U^e, parametrized by the conserved angular momentum p_ϕ.

The contour plots of $U^e(\rho, z)$ provide a vivid picture of the global confinement of charged dust grains. Thus, the critical points of U^e locate the circular orbits, nonequatorial as well as equatorial. Standard methods then yield Lyapunov (nonlinear) stability boundaries [9] in a two-dimensional parameter space, to be described below. Moreover, the stable equilibria form the centers of potential wells, which can contain large populations of particles. These potential wells have their own topological structures, so that a particle which loses *local* stability may still be trapped *globally*. Knowledge of local and global bifurcations for the four basic cases (positive or negative charge, prograde or retrograde orbits) allows one to predict the possible constituents of "halo" orbits, i.e., those that encircle the planet entirely above or below the equatorial plane. Positively charged grains are found to possess stable nonequatorial orbits, both prograde and retrograde, for a wide range of charge-to-mass ratio q/m. Negatively charged grains, on the other hand, form stable halo orbits only for very small grains at very high latitudes.

For a spherical dust grain of uniform density ρ_m (g/cm^3), radius a_μ (microns), and a surface potential of Φ (volts),

$$\frac{q}{m} = \frac{10^6 \Phi}{4\pi \rho_m a_\mu^2} \text{ esu/g}. \tag{1}$$

We shall take $\rho_m = 1$ g/cm^3. Typical values of Φ for Jupiter and Saturn lie in the range $-20 < \Phi < +10$ V [7]. For a given planet and equilibrium radius, stability depends on q/m alone, conveniently measured by the parameter $\hat{\Phi} = \Phi/a_\mu^2$, which we express as a pure number. Since the potential is determined by the ambient plasma, $\hat{\Phi}$ depends only on the grain radius a_μ. An upper bound on $\hat{\Phi}$ is thus a lower bound on a_μ, forming a sort of dynamical sieve. Roughly speaking, grains with $a_\mu > 1$ are gravity dominated, while those with $a_\mu < 1$ are dominated by electromagnetic forces.

Hamiltonian model.—Our starting point is the inertial frame Hamiltonian, in Gaussian units and cylindrical coordinates (ρ, ϕ, z)

$$H = \frac{1}{2m}(p_\rho^2 + p_z^2) + \frac{1}{2m\rho^2}\left(p_\phi - \frac{q}{c}\Psi\right)^2 + U + \frac{q\Omega}{c}\Psi, \tag{2}$$

where $p_\phi = m\rho^2\dot{\phi} + q\Psi/c$ is the conserved angular momentum, $U(\rho, z)$ is the gravitational potential, and $\Psi(\rho, z) = \rho A_\phi$ is the stream function. The induced electric field can then be written $\mathbf{E} = \frac{1}{c}\Omega\nabla\Psi$, where Ω is the planetary spin rate. Notice that the electric field is meridional and everywhere normal to the magnetic field. For Keplerian gravity $U = -\mu m/r$, where $r = \sqrt{\rho^2 + z^2}$ and $\mu = GM_p$. For a centered dipole $\Psi = \mathcal{M}\rho^2/r^3$, with dipole strength $\mathcal{M} = B_0 R_p^3$, where B_0 is the magnetic field strength *on the planetary equator* and R_p is the planetary radius. Thus

$$H = \frac{1}{2m}(p_\rho^2 + p_z^2) + U^e(\rho, z) \tag{3}$$

with effective potential

$$U^e = \frac{1}{2m\rho^2}\left(p_\phi - \frac{\gamma\rho^2}{r^3}\right)^2 - \frac{\mu m}{r} + \frac{\Omega\gamma\rho^2}{r^3}, \tag{4}$$

where now $p_\phi = m\rho^2\dot{\phi} + \gamma\rho^2/r^3$ and $\gamma = q\mathcal{M}/c$ measures the relative strength of the dipole field.

Measuring ρ and z in units of R_p, (4) becomes

$$U^e = \frac{1}{2\rho^2}\left(p_\phi - \frac{\omega_c\rho^2}{r^3}\right)^2 - \frac{\omega_k^2}{r} + \frac{\Omega\omega_c\rho^2}{r^3} \tag{5}$$

with scaled angular momentum $p_\phi = \rho_0^2\dot{\phi} + \omega_c\rho_0^2/r_0^3$. Here $\omega_c = qB_0/mc$ and $\omega_k = \sqrt{\mu/R_P^3}$ are the cyclotron and Kepler frequencies, both evaluated at a point on the planetary equator. For Saturn $R_p = R_s = 60\,300$ km, $M_s = 5.688 \times 10^{26}$ kg, $B_0 = 0.210$ G, and $\Omega = 1.691 \times 10^{-4}$ rad/s [7], so that $\omega_k = 4.160 \times 10^{-4}$ rad/s.

Equilibria.—Equilibria (ρ_0, z_0) are given by $U_\rho^e = U_z^e = 0$, where subscripts denote partial derivatives. For equatorial equilibria ($z_0 = 0$), $p_\phi = \rho_0^2\omega + \omega_c/\rho_0$, so that the radial equation yields a quadratic in ω:

$$\rho_0^3\omega^2 - \omega_c\omega - (\omega_k^2 - \omega_c\Omega) = 0 \tag{6}$$

whose solutions are given by

$$2\rho_0^3\omega_{1,2} = \omega_c \pm \sqrt{\omega_c^2 + 4\rho_0^3(\omega_k^2 - \omega_c\Omega)}. \tag{7}$$

For positive charge ($\omega_c > 0$) there are three possibilities:

(i) $\omega_c\Omega < \omega_k^2$ (Keplerian regime), $\omega_1 > 0$, $\omega_2 < 0$;
(ii) $\omega_c\Omega > \omega_k^2$ (magnetic regime), $\omega_1, \omega_2 > 0$;
(iii) $\omega_c\Omega = \omega_k^2$ (transition case), $\omega_1 = \omega_c$, $\omega_2 = 0$.

We shall refer to the ω_2 branch as "semiretrograde," as it is retrograde only for large q/m. In the magnetic case there is a cutoff when $\omega_c^2 = 4\rho_0^3(\omega_c\Omega - \omega_k^2)$, which is itself a quadratic in ω_c. It is easily seen that this inner quadratic has real roots only for $\rho_0 > (\omega_k/\Omega)^{2/3}$, i.e., the synchronous radius, ρ_s. A "magnetic stopband" exists for $\rho_0 > \rho_s = 1.822R_s$, forming two disjoint loci, as shown in Fig. 1. In addition, case (iii) reveals the existence of a *static* equilibrium, which will prove to be unstable. For negative charge, replacing ω_c with $-\omega_c$ in (7) shows that there is only one case to consider; $\omega_1 > 0$, $\omega_2 < 0$. In contrast to positive charge, there is no cutoff; a pair of prograde-retrograde orbits exist everywhere on the equatorial plane. Figure 1 plots ω_1/ω_k and ω_2/ω_k for $\rho_0 = 1.5$ and 2.0 (inside and outside ρ_s) as functions of ω_c/ω_k for both positive and negative charge. Note that when $\omega_c \to 0$, $\omega_1 \to \omega_k/\rho_0^{3/2}$, the local Kepler frequency. For $\rho < \rho_s$, in the limit of large positive q/m, $\omega_1 \to \omega_c/\rho_0^3$, the local cyclotron frequency, while $\omega_2 \to \Omega$. These limits are all unstable. For large *negative* q/m, $\omega_1 \to \Omega$, while $\omega_2 \to -\omega_c/\rho_0^3$. The stability of these orbits will be discussed below.

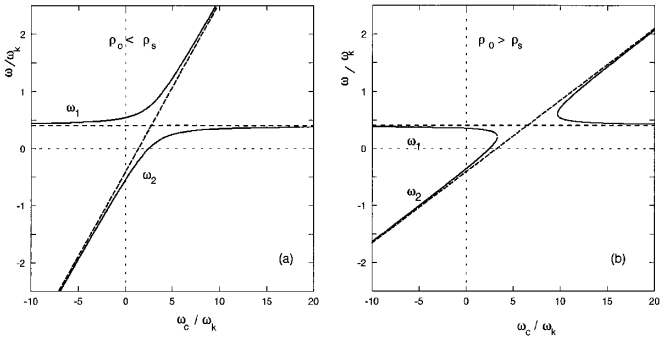

FIG. 1. Orbital frequencies $\omega_{1,2}$ as functions of ω_c/ω_k for (a) $\rho_0 < \rho_s$ and (b) $\rho_0 > \rho_s$. Asymptotes are shown as dashed lines.

Contour plots of $U^e(\rho, z)$ are calculated with p_ϕ referenced to a desired equilibrium orbit at $(\rho_0, 0)$. Figures 2(a) and 2(b) show level sets of U^e for positively

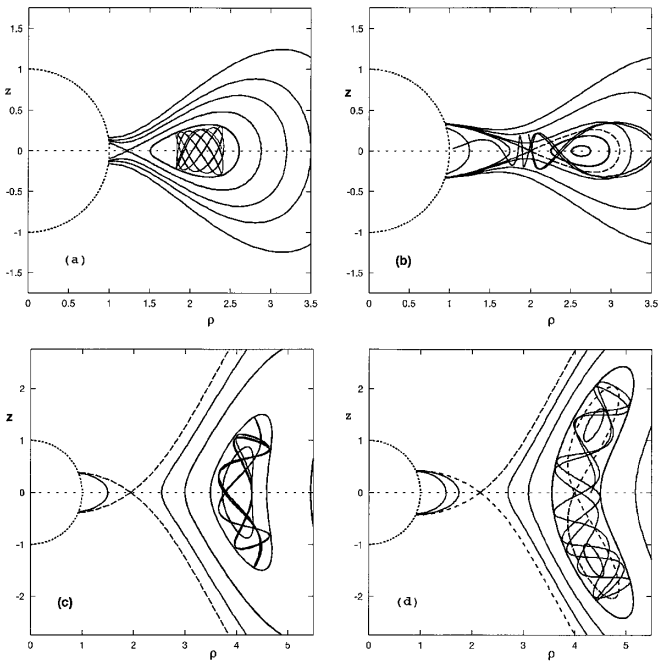

FIG. 2. Contour plots of U^e for positively charged grains in prograde orbits about Saturn, for $\rho_0 = 2R_s$ and (a) $\hat{\Phi} = 400$, (b) $\hat{\Phi} = 650$; and $\rho_0 = 4R_s$, with (c) $\hat{\Phi} = 800$, (d) $\hat{\Phi} = 850$. In the upper pair stability is lost via a tangent bifurcation; in the lower pair an orbit can remain trapped in an outer well even though local stability is lost via a pitchfork bifurcation.

charged grains in prograde orbits about Saturn, with $\rho_0 = 2R_s$. When $\hat{\Phi} = 552.6$ there is a tangent bifurcation, in which the local minimum at $\rho_0 = 2R_s$ becomes a saddle. As can be seen from Fig. 2(b), when $\hat{\Phi} = 650$ nearby orbits are rapidly lost, impacting the planet in a matter of hours. For larger ρ_0 the mode of destabilization is quite different, as depicted in Figs. 2(c) and 2(d) for $\rho_0 = 4R_s$. Here there is a pitchfork bifurcation when $\hat{\Phi} = 817.02$, in which a pair of nonequatorial potential wells is formed. In this case, locally unstable orbits can remain confined within a larger energy surface, as seen in Fig. 2(d) ($\hat{\Phi} = 900$). This clearly illustrates the hazards of relying on local stability thresholds; one must also examine the topology of nearby energy surfaces.

Stability.—An equatorial equilibrium is Lyapunov stable [9,10] if both $U^e_{\rho\rho}, U^e_{zz} > 0$. Explicit stability boundaries may be found by eliminating ω between $U^e_\rho = 0$ and $U^e_{\rho\rho}, U^e_{zz} = 0$ at an equilibrium point. The results are, for positively charged grains in prograde orbits ($\omega = \omega_1$),

$$U^e_{\rho\rho} = 0: \qquad \rho_c = \frac{(5 + 3\sqrt{3})^{1/3}\xi^{2/3}}{(1 - \Omega\xi/\omega_k)^{1/3}}, \tag{8}$$

where $\xi = \omega_c/\omega_k < \omega_k/\Omega$ and

$$U^e_{zz} = 0: \qquad \rho_c = \frac{6^{1/3}\xi^{2/3}}{(1 - 3\Omega\xi/\omega_k)^{2/3}}, \tag{9}$$

where $\xi < 3\omega_k/\Omega$. The algebraic details and corresponding results for nonequatorial equilbria will be reported elsewhere [8]. The stability boundaries $\rho_c(\xi)$ for positive charge are plotted as the solid curves in Fig. 3(a). The stable region is the area to the left of these two curves, which intersect at the point

$$\xi^* = \left(\frac{5 - 2\sqrt{3}}{3}\right)\frac{\omega_k}{\Omega}, \qquad \frac{\rho^*}{R_s} = \left(\frac{19 + 8\sqrt{3}}{6}\right)^{1/3}\left(\frac{\omega_k}{\Omega}\right)^{2/3}. \tag{10}$$

For Saturn $\omega^*_c/\omega_k = 1.259$ ($\hat{\Phi}^* = 939.8$), and $\rho^* = 3.212R_s$, which lies beyond the orbit of Mimas, in the E-Ring. Thus, as $\hat{\Phi}$ is increased, for $\rho < \rho^*$ the radial stability boundary is encountered first, while for $\rho > \rho^*$ the transverse stability boundary is crossed first. This accounts for the metamorphoses of the contour plots observed in Fig. 2. Note that there are no stable equatorial equilibria at all for $\hat{\Phi} > 939.8$. Also note that the transverse stability boundary approaches $\rho_\infty/R_s = (2/3)^{1/3}(\omega_k/\Omega)^{2/3} = 1.592$ for large q/m.

Interesting things happen near the intersection point. Figure 4 shows a contour plot for $\rho = 3.212$ and $\hat{\Phi} = 939.8$, revealing coexisting equatorial and nonequatorial wells, along with a typical trapped halo orbit. The appearance and disappearance of these intricate structures can be accounted for by careful examination of the full Hessian matrix [8].

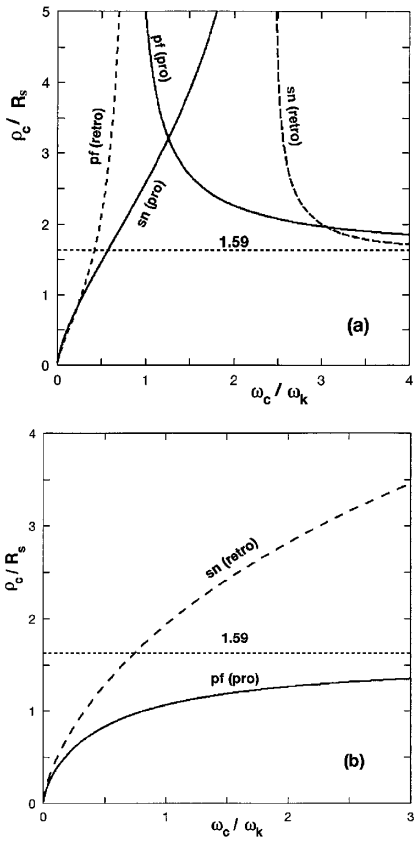

FIG. 3. Stability diagram for equatorial orbits about Saturn for (a) positive charge and (b) negative charge. Boundaries for saddle-node (tangent) bifurcations are labeled "sn," while those for pitchfork bifurcations are labeled "pf."

For semiretrograde orbits ($\omega = \omega_2$) the results are

$$U^e_{\rho\rho} = 0: \qquad \rho_c = \frac{(3\sqrt{3} - 5)^{1/3}\xi^{2/3}}{(\Omega\xi/\omega_k - 1)^{1/3}}, \tag{11}$$

where $\xi > \omega_k/\Omega$ and

$$U^e_{zz} = 0: \qquad \rho_c = \frac{6^{1/3}\xi^{2/3}}{(1 - 3\Omega\xi/\omega_k)^{2/3}}, \tag{12}$$

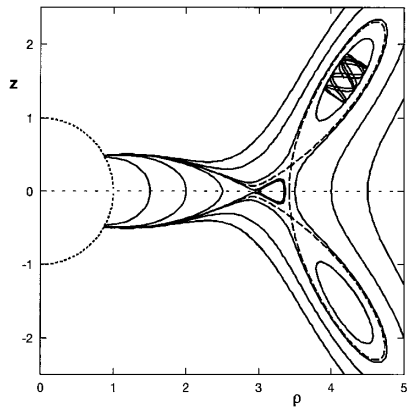

FIG. 4. Contour plot of U^e for positively charged grains in prograde orbits about Saturn near the doubly degenerate point. A halo orbit is depicted in the upper potential well.

where $\xi < 3\omega_k/\Omega$. Static equilibria ($\omega_2 = 0$) are unstable to transverse perturbations. The stability boundaries for positive retrograde orbits are shown as the dashed curves in Fig. 4(a). The stable region is the region to the left of the leftmost $U^e_{zz} = 0$ curve. For $\rho > \rho_s$ a second stable region exists for very large ξ, owing to the fact that both the $U^e_{\rho\rho} = 0$ and $U^e_{zz} = 0$ boundaries attain local minima. In this region both ω_1 and ω_2 are prograde; the slower mode is stable for $\hat{\Phi} > 10\,000$. For a plasma potential of 10 V this corresponds to dust grains smaller than $a \approx 30$ nm (corresponding to about 200 elementary charges).

Now consider negative charge ($\omega_c < 0$). Taking $\xi = -\omega_c/\omega_k$, the transverse stability boundary (9) becomes

$$\rho_c = \frac{6^{1/3}\xi^{2/3}}{(1 + 3\Omega\xi/\omega_k)^{2/3}}. \tag{13}$$

It can be shown that only prograde orbits can reach this stability boundary; retrograde orbits are always stable to transverse perturbations. Similarly, the radial stability boundary is given by (8) with $\xi = -\omega_c/\omega_k$:

$$\rho_c = \frac{(5 + 3\sqrt{3})^{1/3}\xi^{2/3}}{(1 + \Omega\xi/\omega_k)^{1/3}} \tag{14}$$

which turns out to be the stability boundary for retrograde orbits. Prograde negative particles are everywhere stable to radial perturbations. Figure 3(b) depicts the stability boundaries for negative charge. Prograde orbits are stable everywhere above the lower curve ($U^e_{zz} = 0$), while retrograde orbits are stable everywhere above the upper curve ($U^e_{\rho\rho} = 0$). These results agree with those of Northrop and Hill [1] for prograde negative charge but differ essentially from those of Mendis *et al.* [3], who neglect transverse perturbations. While Xu and Houpis [4] carry out a three-dimensional perturbation analysis, their approach focuses on finding equilibria near a given point, rather than deriving explicit stability boundaries.

Figure 5 presents contour plots for negatively charged grains in prograde orbits about Saturn, for $\rho_0 = 1.5$ and $\hat{\Phi} = 2000$ and 8000. Here stability is lost via an *inverse* pitchfork bifurcation, as predicted by (14). For $\rho_0 > 1.592$ all prograde equatorial orbits are stable. For retrograde orbits stability is lost via a tangent bifurcation, in a manner similar to that seen in Fig. 2 for positive prograde orbits. We are currently carrying out a full stability analysis for halo orbits [8]. Preliminary results indicate that, while stable nonequatorial equilibria are easily found for positively charged grains, negatively charged grains form stable halos only for very small particles at high latitudes.

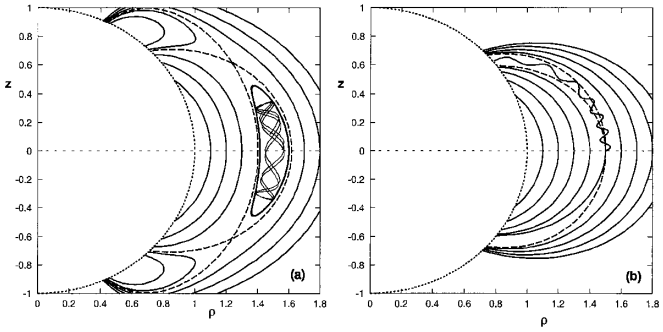

FIG. 5. Contour plots of U^e for negatively charged grains in prograde orbits about Saturn, with $\rho_0 = 1.5R_s$ and (a) $\hat{\Phi} = 2000$ and (b) $\hat{\Phi} = 8000$. When $\hat{\Phi} = 6500$ the elliptic critical point at $\rho_0 = 1.5$ destabilizes in an inverse pitchfork bifurcation. As no outer potential well exists nearby orbits are lost to the planet.

We are grateful to Holger Dullin for helpful discussions. This work was supported by NASA Grants No. NAG5-4163 and No. NAG5-4343.

[1] T. G. Northrop and J. Hill, J. Geophys. Res. **87**, 6045 (1982).
[2] E. Grüen, G. E. Morfill, and D. A. Mendis, in *Planetary Rings*, edited by R. Greenberg and A. Brahic (University of Arizona Press, Tuscon, 1984).
[3] D. A. Mendis, J. R. Hill, W.-H. Ip, C. K. Goertz, and E. Grüen, in *Saturn*, edited by T. Gehrels and M. Matthews (University of Arizona Press, Tuscon, 1984).
[4] R.-L. Xu and L. F. Houpis, J. Geophys. Res. **90**, 1375 (1985).
[5] L. Schaffer and J. A. Burns, J. Geophys. Res. **100**, 213 (1995).
[6] D. Hamilton, Icarus **101**, 244 (1993).
[7] M. Horányi, Annu. Rev. Astron. Astrophys. **34**, 383 (1996).
[8] M. Horányi, H. R. Dullin, and J. E. Howard (to be published).
[9] V. I. Arnold, *Mathematical Methods of Classical Mechanics* (Springer, New York, 1980), 2nd ed.
[10] J. E. Howard, Celest. Mech. **74**, 19 (1999).